SPIE.SPOTLIGHT

# Carbon Nanoparticles in Photoacoustic Imaging

**Ti Zhang** and **Huizhong Cui**

# Carbon Nanoparticles in Photoacoustic Imaging

by Ti Zhang and Huizhong Cui

doi: http://dx.doi.org/10.1117/3.2197936
PDF ISBN: 9781628416725
epub ISBN: 9781628418309
mobi ISBN: 9781628418316

Published by

SPIE Press
P.O. Box 10
Bellingham, Washington 98227-0010 USA
Phone: +1 360.676.3290
Fax: +1 360.647.1445
Email: Books@spie.org
Web: http://spie.org



Spotlight vol. SL04
Last updated 28 May 2015

SPIE.

# Table of Contents

# SPIE Spotlight Series

Welcome to SPIE Spotlight eBooks! This series of tutorials is designed to educate readers about a wide range of topics in optics and photonics. I like to think that these books address subjects that are too broad for journal articles but too concise for textbooks. We hope you enjoy this eBook, and we encourage you to submit your ideas for future Spotlights online.

Robert D. Fiete, *Series Editor*
Exelis Geospatial Systems

## Editorial Board Members

## 1 Introduction

Photoacoustic (PA) imaging is poised to fill a large gap in clinical imaging; PA imaging can provide resolution far beyond ultrasound and comparable to magnetic resonance imaging or computed tomography, but with a small, relatively low cost device that can fit into a hand-held scanner. PA imaging has great potential for the visualization of physiology and pathology molecularity due to its superior tissue penetration depth and good spatial resolution.[1] Endogenous contrast agents with high optical absorption, such as hemoglobin and melanin, can be imaged with better spatial resolution than with pure optical imaging, and the imaging resolution is not limited by strong light scattering in deep biological tissues. In PA imaging, a short-pulsed laser is used to irradiate the tissue, and a focused ultrasonic transducer then detects the PA waves generated via thermoelastic expansion (Fig. 1). The acquired PA data are used to quantify the optical absorption distribution and then construct the tissue structure. In some situations, when endogenous contrast is unavailable (e.g., solid tumors and lymph nodes), exogenous contrast agents are employed to resolve such a problem. In addition to the improvement in imaging contrast, they can also enhance the imaging depth as they absorb light strongly in the near-infrared range (NIR, also known as an optical window or therapeutic window). Moreover, nanomaterials with strong NIR absorption have great potential to serve as PA contrast agents due to their preferential accumulation in tumor tissue, which is because of the enhanced permeability and retention effect. Nowadays, design of contrast agents that produce a sufficient PA signal in a low concentration is still challenging.

To date, the best existing exogenous contrast agents are based on gold nanoparticles (GNPs), which are potentially toxic in the 30 to 70 nm range that is optimum for PA imaging and suffers from the shape deformation upon high energy laser exposure.[3] Organic dyes are also extensively used in PA imaging, but their small size (<2 nm) leads to their nonspecific distribution to a wide range of tissue, causing a low imaging contrast in the region of interest against surrounding

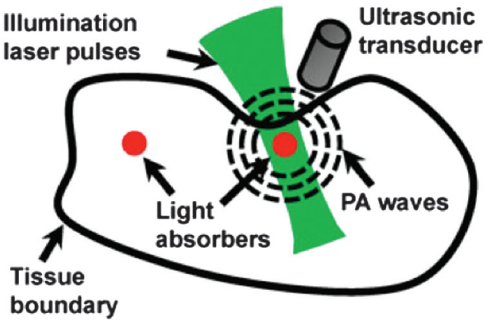


**Figure 1** Illustration of the photoacoustic (PA) effect and PA imaging. Reproduced with permission from Ref. 2. Copyright 2011, John Wiley and Sons.

tissues. In recent years, carbon-based nanocomposites have been developed as PA imaging contrast agents due to their advantages of nontoxicity, photostability, strong NIR absorbance, and easy surface modification.

Among the carbon nanomaterials, carbon nanotubes (CNTs), including multiwall nanotubes and single-wall carbon nanotubes (SWCNTs), were considered, most promising contrast agents because of intrinsic optical absorbance in the NIR and serving as a versatile nanoplatform by coupling with other light-absorbing agents for enhanced or multiplexed PA imaging. Although graphene and graphene oxide (GO) have been demonstrated to be toxic in biological tissues, their stability was greatly enhanced in physiological environments after coating noncovalently with biocompatible polymers or proteins. Consequently, no noticeable *in vitro* toxicity and *in vivo* side effects of GO-based functional nanoparticles were detected. Nanodiamonds (NDs) have failed as optical contrast agents due to their limited optical absorbance in the NIR. However, due to the successful fabrication of the GR1 center in radiation-damaged NDs, most of the energy absorbed upon laser excitation can be translated to heat, and thus generate ultrasonic waves for the use in PA imaging.

This Spotlight summarizes the very recent progress on the surface modifications and applications of carbon nanoparticles as PA contrast agents. It is expected that a PA carbon-based contrast agent modality will have a great potential in basic biomedical research and clinical diagnostic applications.

## 2 Characteristics of Carbon Nanoparticles Used in Biomedical Applications

Carbon allotropes, including graphene or GO, CNTs, and NDs, have shown unique features that are suitable as imaging contrast agents, such as strong NIR absorbance, large surface-to-volume ratio, rigid structure, good thermal conductivity, and the potential for high biocompatibility. In the early stages, their applications were limited by poor aqueous solubility and stability. However, advances in surface functionalization approaches substantially improved the solubility of carbon-based nanoparticles.

Recently, CNTs have been intensively studied as contrast agents in PA imaging systems due to their excellent characteristics. For example, the wide-optical absorption spectrum of CNTs from visible to NIR regions is very useful for providing exogenous PA contrast for detecting tumors, because most of the tumors do not create endogenous PA signals in the NIR region. Moreover, covalent and noncovalent attachment of polyethylene glycol (PEG) on the surface results in CNTs that are highly soluble and stable in a biological environment and allow further surface modification with a contrast enhancer or targeting moiety.[4,5]

Although CNTs can provide strong optical contrast when employed for biomedical applications, their absorption coefficient in the NIR is relatively lower than gold-based nanoparticles. However, thanks to the large surface area, the

NIR optical absorption of CNTs can be improved significantly by conjugating small molecule dyes or coating with a gold layer. Kim and Cui have reported an enhancement of PA contrast by coating CNTs with a golden layer, and demonstrated that CNT-gold hybrids offered a promising alternative for noninvasive detection of cancer.[6,7] Moreover, CNTs can be easily employed for photothermal therapy due to both the strong optical absorption and extraordinary thermal conductivity.

Graphene and its derivatives, such as GO and reduced graphene oxide (rGO), share similar characteristics with CNTs. Compared to CNTs, graphene-based nanomaterials possess a larger surface area and lower aspect ratio. However, graphene nanostructures tend to aggregate in salt or other biological solutions leading to concerns regarding biocompatibility in biological milieus.[8] Therefore, surface modifications to reduce the toxicity and aggregation of graphene-based nanomaterials are required before their use in *in vivo* applications.[9–11] Sheng et al.[9] has reported that bovine serum albumin (BSA), as a native protein, can be used to functionalize rGO to enhance the stability and decrease cytotoxicity in living mice. Eventually, the BSA functionalized rGO was used as a theranostic agent for both PA imaging and photothermal therapy. Carboxylate group functionalized single layer GO sheets have also been synthesized successfully so that a hydrophilic PEG coating could be covalently bound to GO.[7,12–14] The increased biocompatibility by surface modification highlights the physical features of GO as mentioned previously, and thus leads to a broad range of potential applications in biomedicine.

The carbon atoms in NDs are completely sp3 hybridized and have a characteristic tetrahedral configuration, which leads to the physical properties of extreme strength, hardness, and high inertness compared to other nanoparticle forms of carbon. NDs have a very high surface-to-volume ratio, thus their surface-dependent properties are more pronounced than those of bulk diamond. NDs are usually obtained by detonation, plasma-assisted chemical vapor deposition, ultrasound cavitation, and laser ablation techniques. Such prepared NDs contain layers of amorphous and sp2 hybridized carbon, and the resulting surface pattern is determined by the production method and the subsequent purification process. A variety of surface treatments enable biomedical applications of the nanostructured diamonds. For example, hydrogen-terminated NDs exhibit unique properties including tunable electrical conductivity and negative electron affinity, which allows ND to be an electron field emitter.[15,16] Surface modifications via oxidization or gaseous reactants can be applied to produce oxygen containing functional groups, especially carboxyl groups. Such modified NDs can be further modified to improve the solubility of NDs for a variety of specific biomedical applications, such as drug delivery and imaging. Zhang et al.[17] have applied NDs as contrast agents in both *ex vivo* and *in vivo* PA imaging, and it was indicated that NDs were superior to gold nanorods (AuNRs) and SWCNTs based on improved PA amplitude and known low toxicity. In order to enhance the PA signals generated by

NDs, Zhang et al.[18] have demonstrated a significant enhancement of PA emission from fluorescent NDs when they were conjugated with GNPs.

Much effort has been made to synthesize, modify, and optimize carbon-based nanoparticles; the interested reader is referred to Refs. 19–24.

## 3 Applications of Carbon Nanoparticles in Photoacoustic Imaging

The application of a gold coating on CNTs was employed to enhance the NIR absorbance and, therefore, the PA contrast in biomedical imaging. It provides the potential of using PA imaging for highly efficient and selective immune molecular sensing.[7] CNTs were dispersed in hexane to give a concentration of 0.5 mg/mL. One hundred microliters of oleylamine was mixed with 3 mg $HAuCl_4$, and the mixture was added to 2.5 mL of CNTs hexane solution. Finally, 150 mL triisopropylsilane was added to synthesize a gold nanowire GNW-CNT hybrid. To compare the PA contrast of GNW-CNT with other gold and carbon nanoparticles, GNW-CNT hybrids, GNWs, CNTs, and their physical mixture were injected into four tygon tubings with GNW and CNT concentrations of 0.35 and 0.5 mg/mL for PA imaging at an 820-nm laser wavelength. As shown in Fig. 2, the GNW-CNT hybrids exhibited significantly stronger PA signal amplitudes that other forms of nanoparticles. Since PA imaging is an absorption-based technique, the enhancement of PA amplitude results from the increase of optical absorption of the GNW-CNT hybrids. Alpha-fetoprotein (AFP) ELISA Kits purchased from AccuBind were used in PA imaging immune tests. In the treated group, the assigned microwells were treated with AFP at different concentrations for 20 min and washed with phosphate-buffered saline (PBS). Then 0.1 mL of the anti-AFP enzyme reagents conjugated GNW–CNTs were added to each well and incubated for 20 min, followed by the rinse with PBS. In control group 1, only anti-AFP enzyme reagents were added to the AFP-incubated well. In control group 2, bare GNW-CNTs, which were not conjugated with anti-AFP enzyme reagents but were covered with BSA, were added to the AFP-incubated well. The result in Fig. 3 shows that a relatively weak PA signal amplitude can be observed from the controlled wells. However, the anti-AFP enzyme reagents conjugated GNW–CNTs were immobilized on the AFP-pretreated wells, which exhibit apparently increased PA signals. In addition, PA signals from the treated wells increased with the increase in AFP concentration and thus the immobilized amount of GNW–CNTs. This work illustrated the feasibility of using GNW–CNTs as an NIR contrast agent in PA imaging. With a potential application in sensing AFP antigen, it can act as an early cancer indicator with the help of PA imaging.

De La Zerda et al.[25] demonstrated that SWCNTs conjugated with cyclic Arg-Gly-Asp (RGD) peptides to target the $\alpha_v\beta_3$ integrins greatly enhanced the imaging contrast for PA imaging of tumors compared to nontargeted SWCNTs. This group

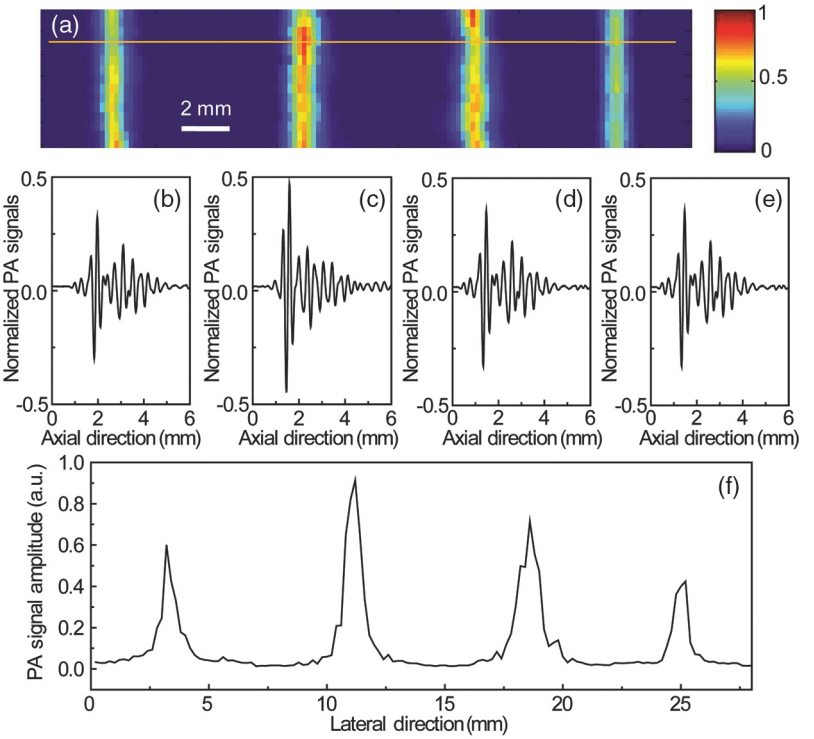


**Figure 2** (a) PA maximum amplitude projection (MAP) image of four particle solutions in tubings from left to right: plain carbon nanotubes (CNTs), CNTs wrapped with gold nanowires (GNWs), CNTs mixed with GNWs, and pure GNWs; (b–e) PA signals from particle solutions; (f) signal profile at the horizontal dashed line position in (a). Reproduced with permission from Ref. 7. Copyright 2013, American Chemical Society.

also developed an ultrahigh sensitive CNT agent by attaching an indocyanine green dye to improve its PA performance, leading to subnanomolar detection of tumors in living mice (Fig. 4).[26] Furthermore, CNTs have also been used as contrast agents in PA mapping of the sentinel lymph node, lymphatic vessels, and PA molecular imaging of glioblastoma tumors and certain cancerous cells.[27–30]

Sheng et al.[9] have developed a protein fabricated nano-rGO to be employed as a diagnostic agent of tumor for *in vivo* PA imaging, and this diagnostic agent showed no noticeable toxic effect with tested doses. In this work, functionalized nano-rGO was prepared by a one-step synthesis using BSA as both a reducing agent and a stabilizer. The UV–visible–NIR absorbance test suggested that the NIR absorbance of nano-GO was enhanced after being reduced by BSA (inset in Fig. 5). This result indicated that nano-rGO could act as a better contrast agent in PA imaging compared to nano-GO. *In vivo* PA imaging was performed in a constructed highly integrated PA/ultrasonic dual imaging modality. BSA functionalized nano-rGO at a concentration of 1 mg/mL was injected to mice bearing

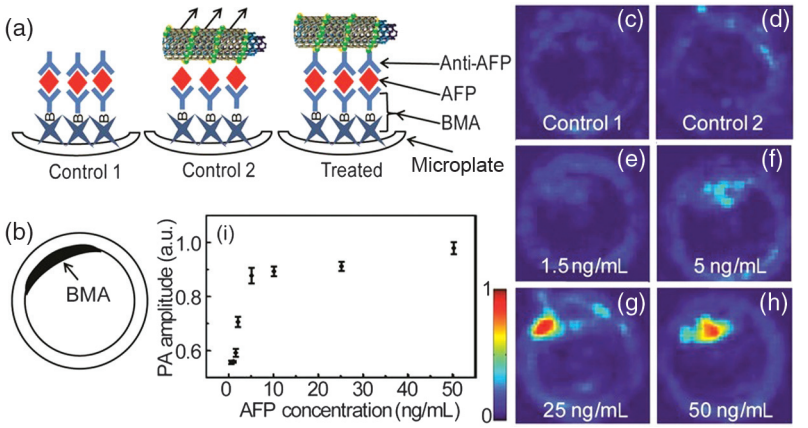


**Figure 3** (a) Schematic image of the controlled and treated methods of immune tests using GNW–CNTs; (b) scheme showing the location of the biotinylated monoclonal antibody (BMA) on the bottom of microplates; (c–d) PA images on controlled microplates; (e–h) PA, images from treated microplates with different alpha-fetoprotein (AFP) concentrations as labeled; (i) PA signal amplitudes from GNW–CNTs as a function of AFP antigen concentration. Reprinted with permission from Ref. 7. Copyright 2013, American Chemical Society.

MCF-7 tumor xenografts (80 $mm^3$ in size) via tail vein. In the PA images, the contrast of the tumor area [green area in Figs. 6(c) and 6(d)] indicated by the accumulated BSA functionalized nano-rGO was significantly enhanced 2-h post-injection. A cytotoxicity 3-(4,5-dimethylthiazol-2-yl)-2,5-diphenyltetrazolium bromide (MTT) assay demonstrated the low toxicity of BSA functionalized nano-rGO.

Nie et al.[31] designed ultrasmall GO nanosheets for both drug delivery to the tumor and signal enhancement in PA imaging of vasculature in the tumor region. In this work, the subtle microvascular changes in the tumor as a response to chemotherapy could be monitored in a timely manner by PA imaging, which benefited from the GO nanosheets' accumulation in the tumor. The PA imaging system revealed the tumor angiogenesis and therapeutic effect much earlier than the morphological measurement by fluorescence imaging because of the better imaging depth and higher spatial resolution of PA imaging. In addition, an imaging probe based on rGO-iron oxide nanoparticle nanocomposite was designed for simultaneous PA imaging and photothermal therapy of cancer.[32]

Nontoxic NDs have been used as a PA imaging contrast agent for deep tissue imaging. The photophysical properties of ion-irradiated NDs were characterized extensively by Fang's group.[32] In a study conducted at the University of Kansas, the feasibility of using radiation-damaged nanodiamonds (DNDs) in PA imaging was studied *ex vivo* and *in vivo*.[17] DNDs were prepared by radiation damaging natural diamond powders with 40-keV $He^+$ ions. The detailed synthetic

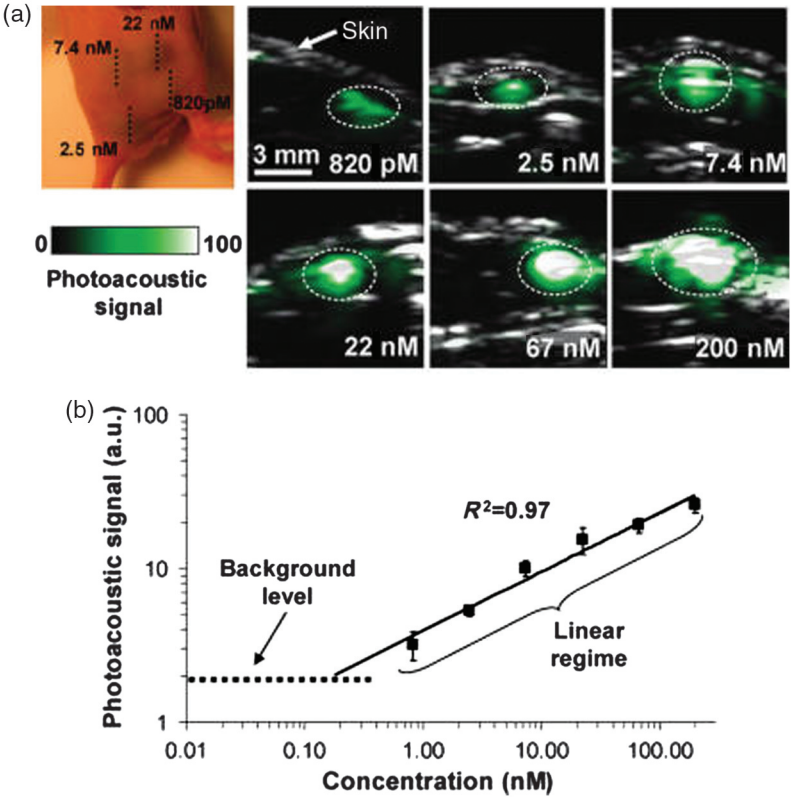


**Figure 4** PA detection of single-wall carbon nanotube-indocyanine green (SWCNT-ICG) in living mice. (a) Mice were injected subcutaneously with SWNT-ICG at concentrations of 0.82 to 200 nM. The images represent the ultrasound (gray) and PA (green) vertical slices through the subcutaneous injections (dotted black line). The skin is visualized in the ultrasound images, while the PA images show the SWCNT-ICG distribution. The white dotted lines on the images illustrate the approximate edges of each inclusion. (b) The PA signal from each inclusion was calculated using three-dimensional regions of interest and the "background" represents the endogenous signal measured from tissues. The error bars represent the standard error ($n = 3$ mice). Linear regression ($R^2 = 0.97$) of the PA signal curve estimates that a concentration of 170 pM of SWCNT-ICG will give the equivalent background signal of tissues. Reprinted with permission from Ref. 26. Copyright 2010, American Chemical Society.

method can be found in a previous work.[11] In this work, a PA microscopy system was employed.[34] In the *ex vivo* study, the DNDs were injected into raw chicken breast tissue for PA imaging (Fig. 7). The optical contrast of the injected area was significantly enhanced by DNDs by 446% compared to the background chicken breast tissue. In the *in vivo* study, the lower back of mice was imaged after subcutaneous injection of DNDs. In Fig. 8, a clear image of the injection site and path was observed with the highest PA signal contrast enhancement of 919%

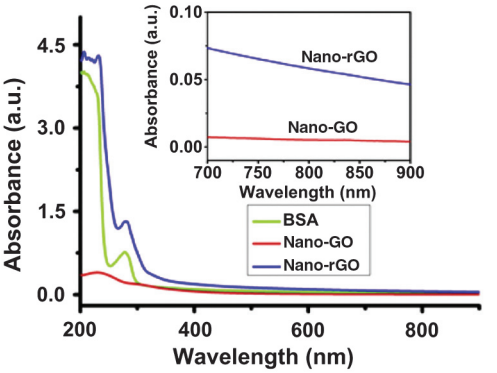


**Figure 5** UV–visible–NIR absorption spectra of bovine serum albumin (BSA), nano-graphene oxide (GO), and nano-reduced graphene oxide (rGO). Reprinted with permission from Ref. 9. Copyright 2013, Elsevier Ltd.

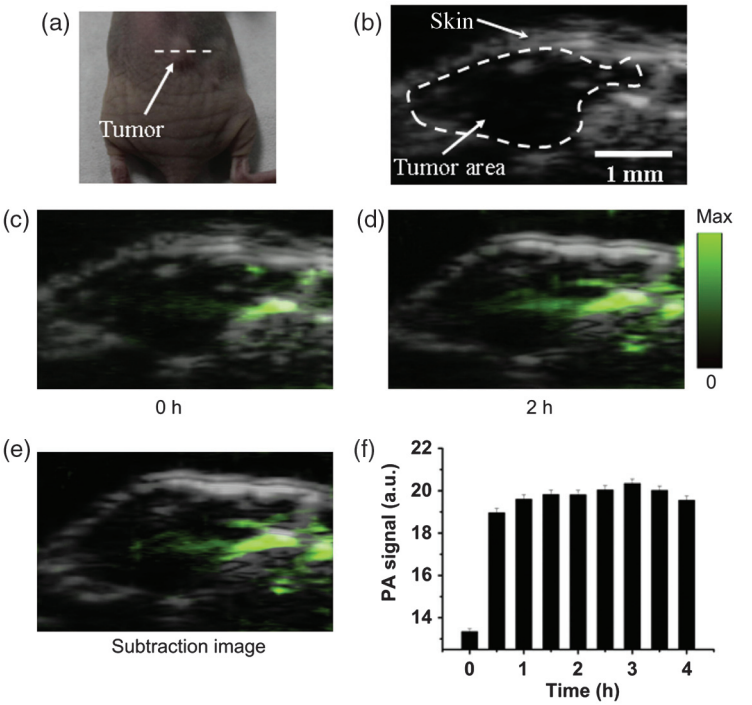


**Figure 6** (a) Digital photo of mice bearing MCF-7 tumor xenografts. (b) Ultrasound (gray) image of the tumor region. (c–e) Ultrasound and PA dual-modality images of the tumor region using nano-rGO as contrast agent. (f) PA signal in the tumor region as a function of the injection time. Reprinted with permission from Ref. 9. Copyright 2013, Elsevier Ltd.

**Table 1** Comparison of photoacoustic (PA) signals between damaged nanodiamonds (DNDs), gold nanorods (AuNRs), and SWNT.

| Particles | Amp (mV)[a] | $C_m$ (mg/mL)[b] | Atom molar concentration (M) | $C_{\mathrm{OKm}}$ (atoms/$L$)[c] | $V_n$ [mV/(atoms/$L$)][d] |
|---|---|---|---|---|---|
| DNDs | $277.9 \pm 11.3$ | 0.04 | $3.33 \times 10^{-3}$ | $2.00 \times 10^{21}$ | $139.0 \times 10^{-21}$ |
| SWNT (970 nm) | $166.9 \pm 5.5$ | 0.04 | $3.33 \times 10^{-3}$ | $2.00 \times 10^{21}$ | $83.4 \times 10^{-21}$ |
| AuNRs (760 nm) | $268.3 \pm 3.6$ | 1.11 | $5.63 \times 10^{-3}$ | $3.39 \times 10^{21}$' | $79.1 \times 10^{-21}$ |
| AuNRs (840 nm) | $281.0 \pm 1.7$ | 1.05 | $5.33 \times 10^{-3}$ | $3.21 \times 10^{21}$ | $87.5 \times 10^{-21}$' |
| Particles | Amp (mV) | $C_m$ (mg/ml) | Particle molar concentration (M) | $C_{\mathrm{particle}}$ (nps/LJ)e | $V_n$ [mV/(nps/$L$)]f |
| DNDs | $277.9 \pm 11.3$ | 0.04 | $1.05 \times 10^{-10}$ | $6.35 \times 10^{13}$ | $44.8 \times 10^{-13}$ |
| SWNT (970 nm) | $166.9 \pm 5.5$ | 0.04 | $3.85 \times 10^{-8}$ | $23.15 \times 10^{15}$ | $7.21 \times 10^{-15}$ |
| AuNRs (760 nm) | $268.3 \pm 3.6$ | 1.11 | $7.09 \times 10^{-9}$ | $4.27 \times 10^{15}$ | $62.8 \times 10^{-15}$" |
| AuNRs (840 nm) | $281.0 \pm 1.7$ | 1.05 | $6.71 \times 10^{-9}$ | $4.04 \times 10^{15}$ | $69.6 \times 10^{-15}$ |

[a]Laser fluence: $18\ \mathrm{mJ/cm^2}$.
[b]Mass concentration.
[c]Calculated by $C_m \cdot N_A / A_f$.
[d]PA signal comparison on an atom basis.
[e]Calculated by $C_m / M_{\mathrm{particle}}$, where $M_{\mathrm{DND}} \sim 0.63$ fg and $M_{\mathrm{AuNR}} \sim 0.26$ fg.
[f]PA signal comparison on a weight basis.

at the injection center. DNDs were also injected ~3 mm into the hip of a mouse and were demonstrated to be visible with an enhanced contrast of 567%. A PA signal amplitude comparison at different absorption wavelengths between DNDs, AuNRs, and SWCNTs was conducted. In Table 1, on an atomic basis, the PA amplitude of DNDs was more than one time stronger than that of AuNRs and SWNTs. On a nanoparticle molar basis, the PA amplitude of DNDs was approximately 70 and 600 times stronger than that of AuNRs and SWNTs, respectively. The author attributed the improvement of PA contrast of DNDs to the high optical absorbance and the high thermal conductivity of DNDs.

DNDs have been conjugated with an anti-human epidermal growth factor receptor 2 (HER2) peptide for breast-cancer-tumor imaging.[35] There were two control groups and one treated group for the *in vivo* PA imaging. In the control

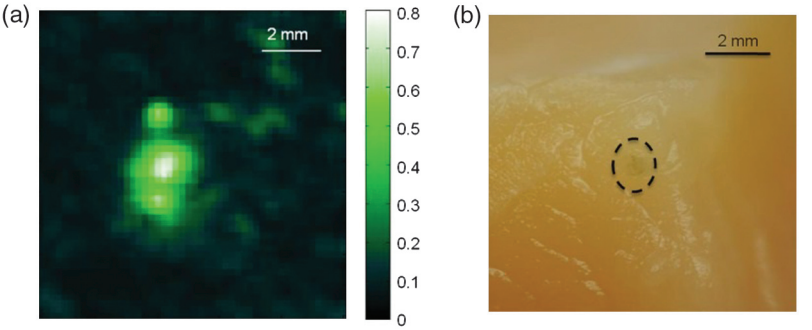


**Figure 7** PA images taken after injecting damaged nanodiamonds (DNDs) into chicken breast tissue. (a) MAP image and (b) corresponding photograph of DNDs in chicken breast tissue (dashed circle).

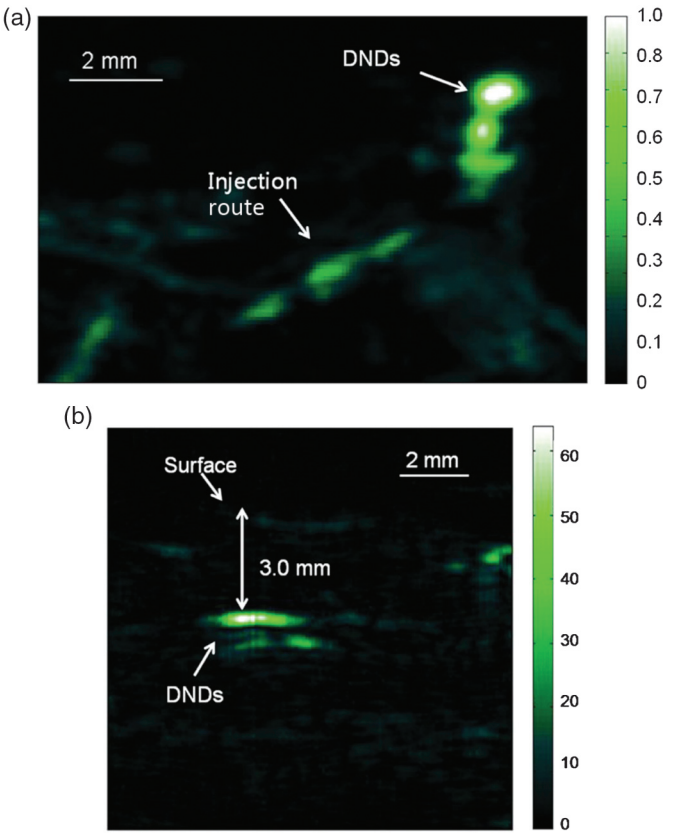


**Figure 8** PA images taken after injecting DNDs subcutaneously at (a) the back (MAP image) and (b) the ventral side of the hip of a mouse (B-scan image).

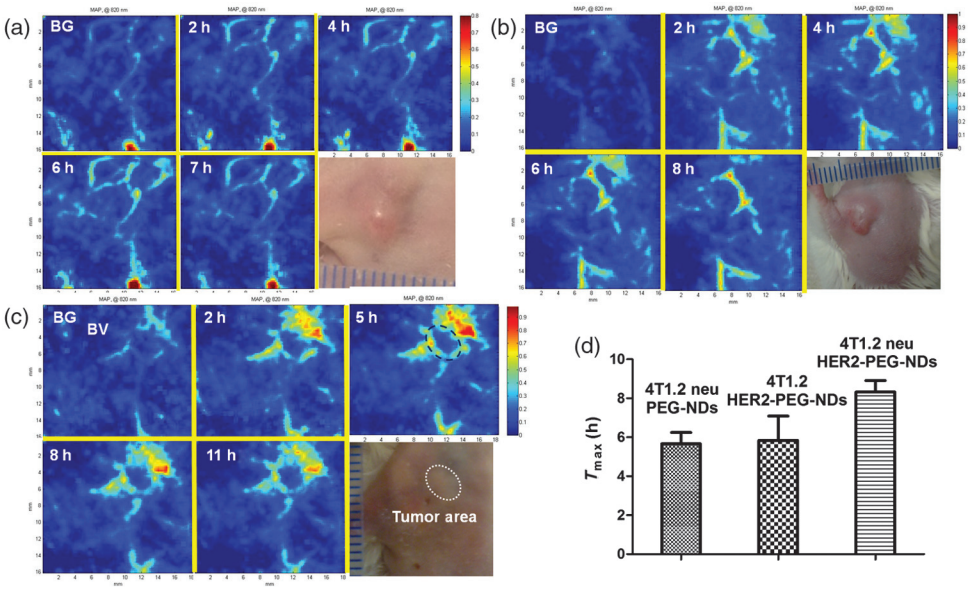


**Figure 9** PA images of the region of interest (ROI) before and at different time points after the injection of nanodiamonds (NDs) and photographs of ROI. (a) 4T1.2 neu tumor model injected with polyethylene glycol-nanodiamonds (PEG-NDs), (b) 4T1.2 tumor model injected with anti-human epidermal growth factor receptor 2 (HER2)-PEG-NDs, (c) 4T1.2 neu tumor model injected with HER2-PEG-NDs, and (d) particle retention time in each group.

groups, the HER2 positive tumor model (4T1.2 neu) and HER2 negative tumor model (4T1.2) were treated with PEG-NDs [Fig. 9(a)] and HER2-PEG-DNDs [Fig. 9(b)], respectively. In the treated group, the HER2 positive breast cancer model is treated with HER2-PEG-NDs [Fig. 9(c)]. As shown in the PA images in Fig. 9, all three groups showed signal enhancement in the tumor region after the intravenous injection of DNDs. However, the slight signal enhancement due to limited accumulation of NDs in the control groups made it difficult to identify the tumor regions. Compared with control groups, a strong contrast was obtained in the treated group so that the solid tumor was outlined completely and clearly. It is demonstrated that the targeting specificity of HER2-PEG-NDs to HER2-receptor is high with the proof of PA images.

## 4 Discussions and Conclusion

Among the three main kinds of carbon nanoparticles employed in PA imaging, NDs exhibit the greatest advantages of chemical inertness and biocompatibility. The safety of carbon nanoparticles is a critical consideration in their development for biological uses. The large surface-to-volume ratio of carbon particles at the nanoscale brings up the importance of surface chemistry. The biocompatibility of carbon nanoparticles is, in part, determined by the surface physical and

chemical properties, including surface chemistry, surface charge, and particle size. The tolerable dose is ultimately limited by their accumulation and elimination from the body, as no known biological process can degrade carbon nanomaterials. Thus, the safety of carbon nanoparticles still needs extensive systemic investigation before their use in humans.

Nowadays, the most attractive exogenous nanoparticle-based PA contrast agent is AuNRs, which have the advantages of high optical absorption and tunable wavelengths with adjustable aspect ratios. However, although no photobleaching occurs on AuNRs upon laser irradiation compared to dye embedded nanoparticles, their rod-like shape tends to deform when exposed to high laser intensity. As a result, AuNRs cannot provide consistent PA signals during diagnosis, and thus are incapable of application into the real-time monitoring of therapeutic effects. However, all the carbon nanoparticles are stable with that morphological structure, thus their optical absorption at a certain wavelength does not change during the procedure of imaging. Other carbon nanoparticles with strong optical absorption, such as carbon nanodots and fullerenes, have also been investigated as PA-imaging contrast agents.[21,36] However, to date, none of the tested particles can be termed as the best exogenous contrast agents for use in PA imaging, since any type of nanoparticles in the blood circulation did not significantly enhance the *in vivo* optical contrast and current PA imaging work is limited. Instead, every proposed nanoparticle must be developed for a specific application.

In conclusion, due to the excellent physical and chemical properties of carbon-based nanoparticles, they have applications in PA-imaging techniques. Particularly, the development of surface modification strategies paves the way for carbon nanoparticles to be applied in biological systems. In addition, receptor-targeted nanoparticles allowed the specific and selective detection of cancer. It can be expected that carbon nanoparticles can be used as molecularly selective contrast agents for PA imaging with high biocompatibility. As a result, they may improve the ability of the PA imaging modality to detect disease at an early stage. Future work may focus on developing multifunctional carbon nanoparticles, such as those used in photothermal therapy, for carbon nanoparticles with high-optical absorption.

## References

1. X. Yang et al., "Photoacoustic tomography of small animal brain with a curved array transducer," *J. Biomed. Opt.* **14**(5), 054007 (2009).
2. J. Yao and L. V. Wang, "Photoacoustic tomography: fundamentals, advances and prospects," *Contrast Media Mol. Imaging* **6**(5), 332–345 (2011).
3. A. Wijaya et al., "Selective release of multiple DNA oligonucleotides from gold nanorods," *ACS Nano* **3**(1), 80–86 (2009).
4. Z. Liu et al., "Supramolecular chemistry on water-soluble carbon nanotubes for drug loading and delivery," *ACS Nano* **1**(1), 50–56 (2007).
5. Z. Liu et al., "In vivo biodistribution and highly efficient tumour targeting of carbon nanotubes in mice," *Nat. Nanotechnol.* **2**(1), 47–52 (2006).

6. S. Zanganeh et al., "Photoacoustic imaging enhanced by indocyanine green-conjugated single-wall carbon nanotubes," *J. Biomed. Opt.* **18**(9), 096006 (2013).
7. H. Cui et al., "Ultrathin gold nanowire-functionalized carbon nanotubes for hybrid molecular sensing," *ACS Nano* **7**(9), 7805–7811 (2013).
8. D. Li et al., "Processable aqueous dispersions of graphene nanosheets," *Nat. Nano* **3**(2), 101–105 (2008).
9. Z. Sheng et al., "Protein-assisted fabrication of nano-reduced graphene oxide for combined in vivo photoacoustic imaging and photothermal therapy," *Biomaterials* **34**(21), 5236–5243 (2013).
10. G. Lalwani et al., "Graphene-based contrast agents for photoacoustic and thermoacoustic tomography," *Photoacoustics* **1**(3–4), 62–67 (2013).
11. G. Goncalves et al., "Surface modification of graphene nanosheets with gold nanoparticles: the role of oxygen moieties at graphene surface on gold nucleation and growth," *Chem. Mater.* **21**(20), 4796–4802 (2009).
12. U. Dembereldorj et al., "Gold nanorod-assembled PEGylated graphene-oxide nanocomposites for photothermal cancer therapy," *Photochem. Photobiol.* **90**(3), 659–666 (2014).
13. H. Shen et al., "PEGylated graphene oxide-mediated protein delivery for cell function regulation," *ACS Appl. Mater. Interfaces* **4**(11), 6317–6323 (2012).
14. Z. Liu et al., "PEGylated nanographene oxide for delivery of water-insoluble cancer drugs," *J. Am. Chem. Soc.* **130**(33), 10876–10877 (2008).
15. D. He et al., "Electron transport and electron field emission of nanodiamond synthesized by explosive detonation," *Diamond Relat. Mater.* **9**(9–10), 1600–1603 (2000).
16. G. Galli, "Structure, stability and electronic properties of nanodiamonds," in *Computer-Based Modeling of Novel Carbon Systems and Their Properties*, L. Colombo and A. Fasolino, Eds., pp. 37–56, Springer, Netherlands (2010).
17. H. Zhang et al., "Tissue-compliant neural implants from microfabricated carbon nanotube multilayer composite," *ACS Nano* **7**(9), 7619–7629 (2013).
18. B. Zhang et al., "Photoacoustic emission from fluorescent nanodiamonds enhanced with gold nanoparticles," *Biomed. Opt. Express* **3**(7), 1662–1629 (2012).
19. K. Kahoe et al., "Large-scale solvothermal synthesis of fluorescent carbon nanoparticles," *Nanotechnology* **25**(39), 395601 (2014).
20. C. Jiang et al., "Plane-interface-induced lignin-based nanosheets and its reinforcing effect on styrene-butadiene rubber," *Express Polym. Lett.* **8**(9), 619–634 (2014).
21. L. Wu et al., "A green synthesis of carbon nanoparticle from honey for real-time photoacoustic imaging," *Nano Res.* **6**(5), 312–325 (2013).
22. Z. Lou et al., "Controlled synthesis of carbon nanoparticles in a supercritical carbon disulfide system," *Materials* **7**(1), 97–105 (2014).
23. H. Li et al., "One-step ultrasonic synthesis of water-soluble carbon nanoparticles with excellent photoluminescent properties," *Carbon* **49**(2), 605–609 (2011).
24. B. Zhang, C.-Y. Liu, and Y. Liu, "A novel one-step approach to synthesize fluorescent carbon nanoparticles," *Eur. J. Inorg. Chem.* **2010**(28), 4411–4414 (2010).
25. A. De La Zerda et al., "Carbon nanotubes as photoacoustic molecular imaging agents in living mice," *Nat. Nano* **3**(9), 557–562 (2008).
26. A. De La Zerda et al., "Ultrahigh sensitivity carbon nanotube agents for photoacoustic molecular imaging in living mice," *Nano Lett.* **10**(6), 2168–2172 (2010).
27. M. Pramanik et al., "In vivo carbon nanotube-enhanced non-invasive photoacoustic mapping of the sentinel lymph node," *Phys. Med. Biol.* **54**(11), 3291–3301 (2009).
28. L. Xiang et al., "Photoacoustic molecular imaging with antibody-functionalized single-walled carbon nanotubes for early diagnosis of tumor," *J. Biomed. Opt.* **14**(2), 021008 (2009).

29. J.-W. Kim et al., "Golden carbon nanotubes as multimodal photoacoustic and photothermal high-contrast molecular agents," *Nat. Nano* **4**(10), 688–694 (2009).
30. F. Zhou et al., "Mitochondria-targeting photoacoustic therapy using single-walled carbon nanotubes," *Small* **8**(10), 1543–1550 (2012).
31. L. Nie et al., "Early-stage imaging of nanocarrier-enhanced chemotherapy response in living subjects by scalable photoacoustic microscopy," *ACS Nano* **8**(12), 12141–12150 (2014).
32. K. Yang et al., "Multimodal imaging guided photothermal therapy using functionalized graphene nanosheets anchored with magnetic nanoparticles," *Adv. Mater.* **24**(14), 1868–1872 (2012).
33. C.-Y. Fang et al., "Preparation and characterization of ion-irradiated nanodiamonds as photoacoustic contrast agents," *J. Nanosci. Nanotechnol.* **15**(2), 1037–1044 (2015).
34. A. J. Andersen et al., "Complement activation by PEG-functionalized multi-walled carbon nanotubes is independent of PEG molecular mass and surface density," *Nanomed. Nanotechnol. Biol. Med*. **9**(4), 469–473 (2013).
35. T. Zhang et al., "In vivo photoacoustic imaging of breast cancer tumor with HER2-targeted nanodiamonds," *Proc. SPIE* **8815**, 881504 (2013).
36. V. Krishna et al., "*Use of fullerenes in photoacoustic imaging*," Google Patents (2011).

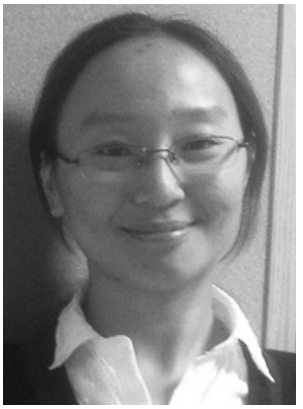

**Ti Zhang** obtained her BS degree in chemistry from Nankai University, Tianjin, China, in 2006, followed by an MS degree in analytical chemistry at the Wuhan University, Hubei, China, in 2008. She joined Dr. Forrest's Group in 2010 and earned a PhD in pharmaceutics and drug delivery at the University of Kansas in 2015. Her research interests include the development of nanomaterials for tumor-targeted imaging, as well as polymeric nanocarriers that deliver anticancer agents exclusively to tumor tissues to improve antitumor efficacy and reduce systemic toxicity.

**Huizhong Cui** joined Huazhong University of Science and Technology in Wuhan, Hubei province and earned a bachelor's degree in mechanical engineering and automation in 2006. He came to the University of Kansas in January 2009 to join Dr. Xinmai Yang's Group to start his research on photoacoustic imaging-guided high-intensity focused ultrasound. He earned his PhD degree in 2012. Since February 2013, he works as a postdoctoral researcher in the Department of Chemistry at the University of Kansas, working on developing new biosensors for immunoassays.